Huygens Probe Entry, Descent, and Landing Dynamics Assessment Using a Multi-Body Parachute Model

Caleb Robb*, Alejandro R. Pensado†, Richard G. Winski‡, James W. Williams*, Michael Manwell*
Analytical Mechanics Associates, Hampton, VA, 23666, USA

The Dragonfly project is a New Frontiers Program mission that is slated to launch in 2028 and deliver a rotorcraft to Titan, Saturn's largest moon. With the launch date approaching, there is an increased focus on the validation and verification of models that are used by the trajectory simulations. One of the models that contributes the most to the uncertainty of the entry, descent, and landing simulation is the atmosphere. Since Huygens is the only mission that has collected in-situ measurements during a descent, a current plan for the validation of the atmosphere model centers around reconciling that flight data with the current atmosphere model used by the Dragonfly flight mechanics team. To complete this, a 6 degree-of-freedom, multi-body simulation has been created using the Program to Optimize Simulated Trajectories 2 (POST2), the prime simulation tool for Dragonfly Entry and Descent, to predict the dynamics of Huygens using the reconciled models. The dynamics predicted by the simulation are then compared to flight data where possible and the previous analysis that was published by the authors last year. Current results show agreement to the available flight data, with an emphasis placed on the metrics that were flagged in the last analysis. The reconciliation is set to continue as areas of concern will be reported and inspected by the model developer.

I. Introduction

SLATED to launch in 2028, the Dragonfly project is a New Frontiers Program mission that is scheduled to land a rotorcraft on Titan in the mid 2030s [1]. The mission concept of operations involves a long descent through the very dense Titan atmosphere, with the majority of that time spent under parachute. The entry, descent, and landing phase is simulated using the Program to Optimize Simulated Trajectories II (POST2) [2]. This platform provides a six degree-of-freedom, rigid-body flight dynamics simulation framework that can extend to multiple-body problems. POST2 allows the user to implement a variety of models including gravity, aerodynamics, mass properties, parachute, and atmosphere. Figure 1 shows an example of the various models used to simulate an EDL flight on Titan using the Dragonfly POST2 simulation. Due to the very long descent for Dragonfly (appx. 2.5 hours), the validation of the atmosphere model in particular is an important step in the lead up to launch.

A validation methodology that has been chosen for the atmosphere model is to compare flight data from Huygens, an ESA mission that collected in-situ data from a descent on Titan in 2005, and data from a simulation based on the models available. The majority of those models are discussed in previous work by this paper's authors [3], which detailed the simulation development and flight dynamics results using a simple parachute model with comparison to Huygens flight data. A gap identified in that analysis was the need to better model the multi-body dynamics of the EDL system, which was done by implementing a multi-body parachute model. The results using the simple parachute model showed good agreement with the overall trajectory, but the model detailed in this paper allowed for a comparison between simulated and recorded attitude dynamics, as well as quantifying parachute performance, all while applying the Dragonfly project's Titan atmosphere model.

*Aerospace Engineer, Atmospheric Flight and Entry Systems Branch, MS 489, AIAA Member.
†Aerospace Engineer, Atmospheric Flight and Entry Systems Branch, MS 489, Senior AIAA Member.
‡Aerospace Engineer, Atmospheric Flight and Entry Systems Branch, MS 489, AIAA Associate Fellow.

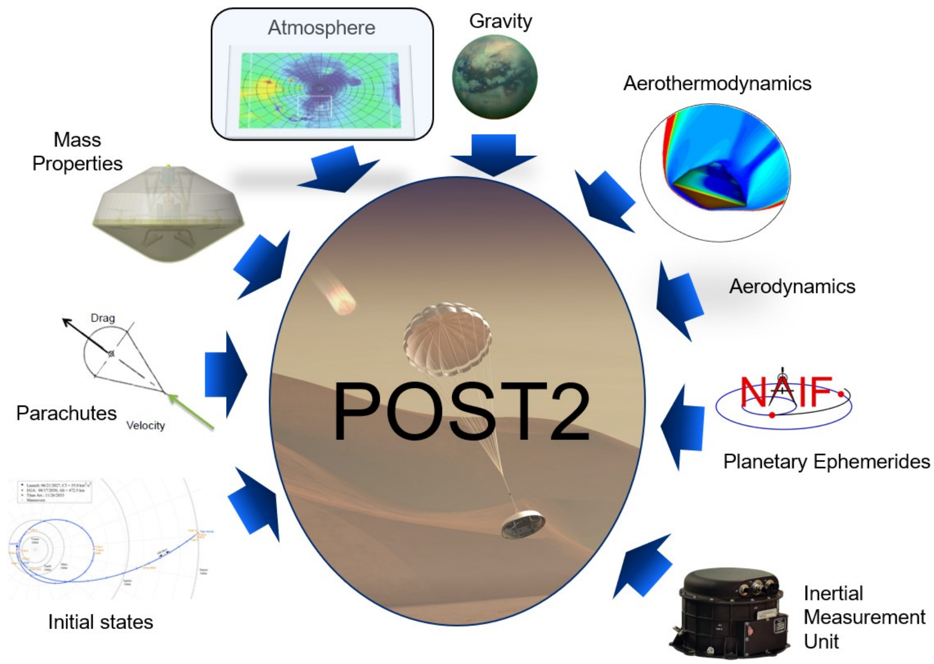

Fig. 1 POST2 Dragonfly Subsystem Model Overview

II. Huygens Concept of Operations

The concept of operations for Huygens is shown in Figure 2 and Table 1, from References [4] and [3] respectively, detailing the sequence which was recreated in the simulation. Notably, the Huygens trajectory was long compared to other interplanetary missions, reaching about two and a half hours, with most of the time spent under parachute. There are three total parachutes used during the Huygens descent, referred to in sequence as the pilot, main, and stabilizer parachutes.

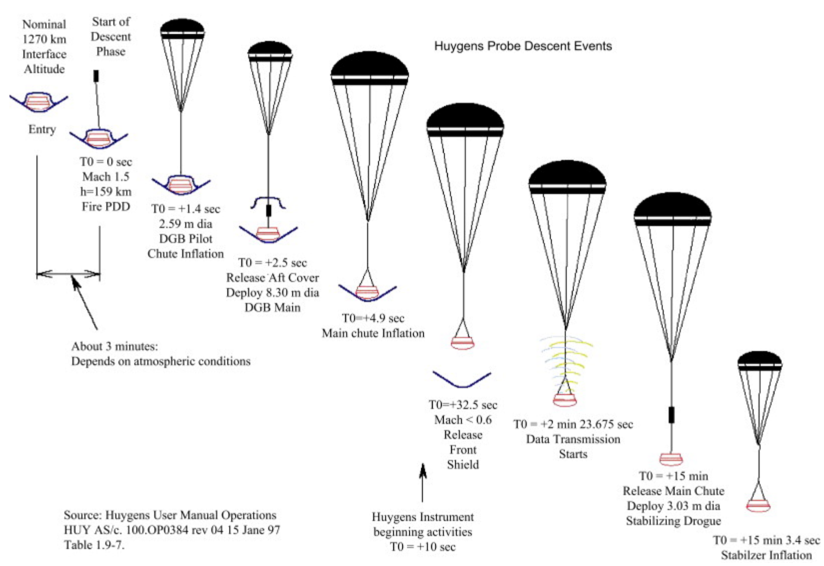

Fig. 2 Huygens EDL Sequence Overview[4]

The EDL sequence for Huygens starts at the entry interface, determined to be 1270 kilometers. The entry vehicle then descends until the acceleration reaches 10 m/s^2 and descending, then a g-trigger starts a 6.5 second timer. When that timer elapses, the mortar for the pilot parachute is deployed. The rest of the EDL sequence is then based on a timer that starts at mortar deployment. Table 1 provides the timings for the event sequence and is based on two anchors: the acceleration-based trigger (AT) and a descent timer (DT) that starts at mortar deployment.

Table 1 EDL Event Sequence based on Reference [3]

Event	Criteria	Value
Entry Interface	Altitude (km)	1270
Pilot Deploy Trigger	Sensed Acceleration (m/s^2)	10
Pilot Deploy	Time AT (s)	6.375
Pilot Inflation	Time DT (s)	1.4
Main Deploy	Time DT (s)	2.5
Main Inflation	Time DT (s)	4.9
Heatshield Jettison	Time DT (s)	32.5
Stabilizer Deploy	Time DT (s)	900
Stabilizer Inflation	Time DT (s)	903.4

III. Modeling and Simulation

This work is an expansion on the work of Ref. [3], and the majority of the models have remained unchanged. Please refer to that paper for references on the entry vehicle and probe aerodynamics, mass properties, and initial conditions, as well as any other models not specifically noted in this paper. An additional reference for some of the models that were used from the Dragonfly project is Ref. [5], which covers some details of the atmosphere and gravity models that were used during this analysis. Even the atmosphere model, whose verification serves as the main driver behind this analysis, remains unchanged in this paper.

The primary effort discussed in this paper is the implementation of the new, higher-fidelity parachute model, outlined in Sec. III.A. Each of the parachutes used by Huygens were disk-gap-band parachutes with geometric properties found in Reference [6]. The coordinate system shown in Figure 3 is the reference point for the mass properties and the locations shown in Tables 2 and 3.

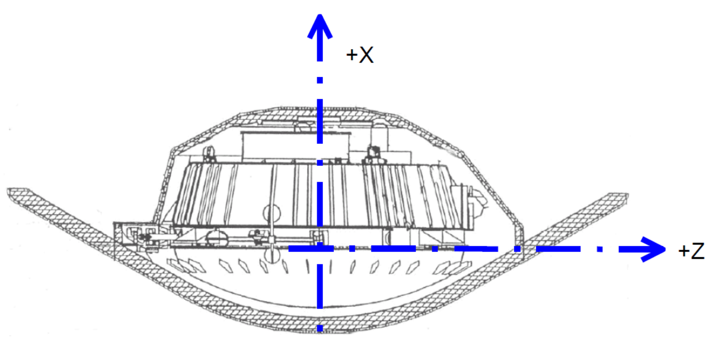

Fig. 3 Huygens Mass Properties Reference Point [6]

A. Parachute Model

A finding in the last paper was that a more complicated parachute model could be used to isolate the dynamics that were flagged by the authors as possibly artificial, and possibly match dynamics of the probe to the available flight data. The previous work utilized a simplified parachute model, with the parachute modeled as a drag force applied at the triple bridle confluence point, visualized in Figure 4. A multi-body parachute model treats everything above the triple bridle confluence point as a separate body from the entry vehicle, with the bridle lines connecting that body to the entry vehicle. That necessitates much more detailed models but gives more insight into the dynamics of the system.

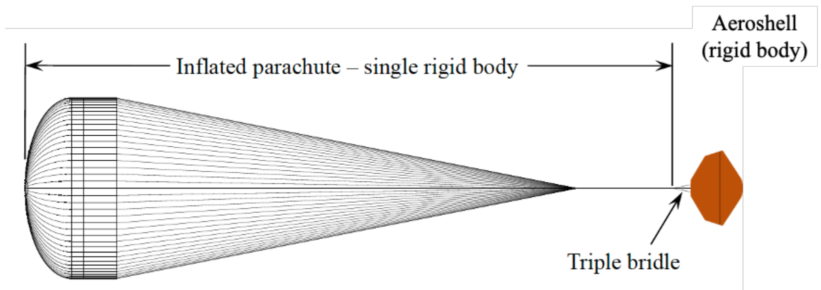

Fig. 4 Parachute Geometry (Not to Scale)

The key locations for the model are summarized in Table 2. The vertical component of the bridle attachment plane, the height of the triple bridle, and the location in the Huygens frame, which was presented in Fig. 3, are all added to the table.

Table 2 Triple bridle confluence point definition along the X Huygens Frame as shown in Fig. 3 from Reference [6]

Parachute	Bridle Attachment (m)	Bridle Height (m)	Bridle Confluence Point in Huygens Frame (m)
Pilot	0.5572	0.53	1.0872
Main	0.4468	3.88	4.3268
Stabilizer	0.3755	3.88	4.2555

1. Multi-Body Implementation

The methodology for the multi-body implementation is very similar to the model used by the 2012 Mars Science Laboratory (MSL) [7] lander and in ASPIRE [8], which, similar to Huygens, had a parachute attached with a riser and a triple bridle confluence point. In the multi-body model, the parachute acts as a separate, six degree-of-freedom body that is connected to the entry vehicle through the triple bridle. Everything above the triple bridle is assumed to be a rigid body after inflation, with the force transferring through the triple bridle confluence point. At that point, the effects of the parachute are translated through the three bridle legs, modeled as three tension-only spring damper systems, Eq. 1.

$$F_{bridleleg} = k\Delta L + c\frac{d(\Delta L)}{dt} \tag{1}$$

where the k value and c values are the line stiffness and damping terms, respectively, that have been found experimentally for the lines used by the Dragonfly project [5]. Although those lines are the same material as those used by Huygens, the uncertainty around composites and the configuration of the lines used by Huygens led to some tuning in the specific numbers to match the flight data available. The assumed values for the stiffness and damping are 9.5E4 and 6.15E2 respectively. The lines are then applied at attachment points listed in Ref [6].

For the simple parachute model, Table 2 has the key parameters; however, for the multi-body model, more information is necessary. Namely, the location of the connection points in every axis, which are covered in Table 3. The connection points are where the bridle leg connects to the probe, with the other point being the parachute's triple bridle confluence point.

2. Parachute Aerodynamics

The aerodynamics of the parachute that is used in this analysis is based on the Dragonfly model for the drogue parachute, which is a disk-gap-band parachute. The static aerodynamics model was originally based off of the formulation

Table 3 Triple bridle Attachment Points

Parachute	Bridle Attach Vertical Distance (m)	Bridle Attach Location y (m)	Bridle Attach Location z (m)
Pilot Leg 1	0.5572	0.0866	0.05
Pilot Leg 2	0.5572	-0.0866	0.05
Pilot Leg 3	0.5572	0.0	-0.1
Main Leg 1	0.4468	0.0	-0.47577
Main Leg 2	0.4468	0.41203	0.23789
Main Leg 3	0.4468	-0.41203	0.23789
Stabilizer Leg 1	0.3755	-0.16656	-0.45762
Stabilizer Leg 2	0.3755	0.47959	0.08457
Stabilizer Leg 3	0.3755	-0.131303	0.37306

in Ref. [9], created for a Mars parachute system. The Dragonfly parachute aerodynamics were tuned to account for the difference in parachute canopy properties, listed in Table 4.

Table 4 Parachute Geometric Properties

Parachute	Geometric Porosity	Diameter (m)
Dragonfly Drogue	12.5%	8.25
Huygens Pilot Parachute	13.1%	2.59
Huygens Main Parachute	22.4%	8.3
Huygens Stabilizer Parachute	22.4%	3.03

Tuning was conducted to account for differences in the canopy geometry, specifically the geometric porosity and gap-band ratio. The specifics of the Huygens parachute's aerodatabase are a large source of uncertainty in the results. The documentation for the Huygens descent, Ref. [6], focuses on the drag coefficient. With the multi-body model, a more elaborate aerodatabase is necessary, with coefficients for forces and moments in each axis. This led to the use of the Dragonfly drogue parachute's aerodatabase in this study, with the static aero coefficients tuned so that the bulk performance reasonably matched Huygens observables, e.g. the descent time.

3. Parachute Inflation Model

The parachute inflation model used for this analysis is similar to the model used by MSL [7]. The bag is ejected by a mortar, whose force model is a scaled version of that used by the Dragonfly project, and the time to line stretch is estimated using the muzzle velocity of the projectile bag. An important note is that, although the force of the mortar is modeled, the bag does not see any aerodynamic forces. When the bag of the parachute reaches the line stretch length, the separate parachute vehicle is first initiated and the mass properties and aerodynamics of the parachute become active. The next event, full inflation, is then based on a timer. More information over the nuances of that model are available in the Reference [7].

4. Parachute Apparent Mass

The parachute model also includes an apparent mass model, the same as used by MSL and Mars 2020, whose performance is described in Reference [10]. This model consists of a point mass acting at the physical center of mass of the parachute. The apparent mass, m_A, represents the entrained air in the parachute canopy, with the model aimed at modeling the inertia of that mass. The mass itself is a product of the density of the fluid at the parachute center of mass and the reference diameter of the parachute, shown in Equation 2.

$$m_A = K_A \pi \rho_\infty D_0^3 \tag{2}$$

The goal of the apparent mass model is to model the inertia of the entrained mass of the fluid within the canopy. In this model, that takes the form of a force that works opposite of gravity with the magnitude computed in Equation 3. The apparent mass proportionality term, K_A, is a tuned quantity in this study due to a lack of data from Huygens documentation to compute that value. As a notable distinction, the apparent mass term does not add mass the system, it is only calculated to be applied in Equation 3. The term being calculated, F_B, is the force output of the model to balance the effect of the added intertia from the entrained mass.

$$F_B = m_A g \tag{3}$$

Due to the environment on Titan, low gravity and high atmospheric density, the system shows a large sensitivity to this model. The high density leads to a higher inertia, modeled as a force resisting the gravitational acceleration of the system. The ratio of that force to the probe weight leads to a high impact on the trajectory. Tuning of the K_A term, which is an unknown, was conducted in tandem with the static aerodynamics of the parachute to match the overall trajectory time of descent. Further work could be conducted to derive the K_A term instead of using an assumed value.

B. Atmosphere Model

The atmospheric parameters have remained unchanged since the previous paper in this series. The model specifies minimum, nominal, and maximum profiles for the winds, temperature, and density as a function of altitude. The profiles are largely based on work detailed in Reference [11] and analysis conducted on the Huygens flight data. The zonal wind profile shown in Figure 5(a) contains features at 100, 80, 70, and 60 kilometers that were noted as introducing possible artificial dynamics into the system.

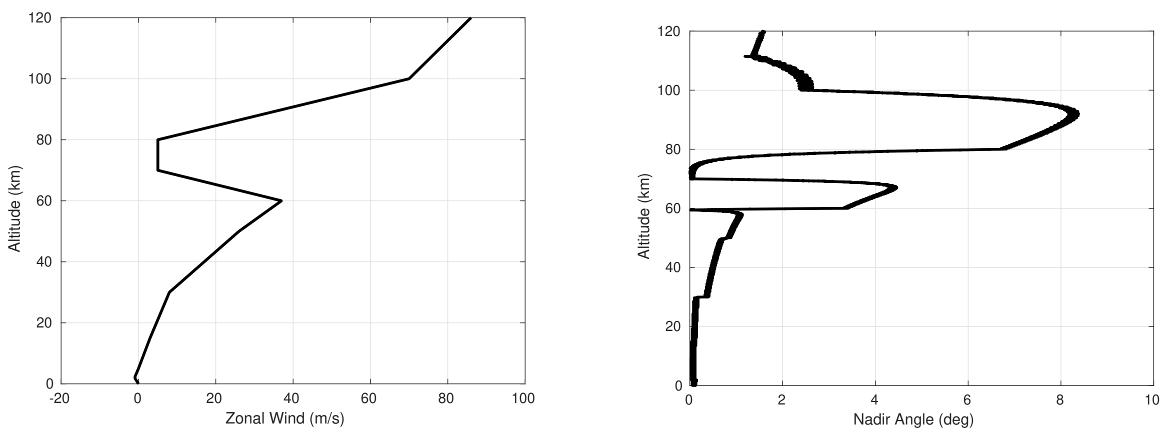

(a) Zonal Wind Profile

(b) Nadir Angle Profile

Fig. 5 Effect of Zonal Wind Profile on the Nadir Angle

The nadir angle is used in Figure 5 due to how clear the effects of the zonal wind can be seen. The large elevations of nadir angle due to changes in the slope of the wind profile are considered to be possibly artificial in nature. The multi-parachute model is used to increase the fidelity of the dynamics simulation to isolate the reason for those high, subsisting nadir angles to the zonal wind profile.

IV. Results

This paper's primary focus is to investigate the behavior shown in Figure 5, which was noted in previous analysis as being possibly an artifact of the zonal wind profile. The methodology taken in this paper is to add a multi-body parachute model and compare the results to available flight data and previous results. Additionally, a more complicated parachute model allows for a better prediction of attitudes and attitude rates during descent, as well as the ability to predict parachute dynamics.

A. Flight Data Comparison

The data products from Huygens that are able to be readily compared are the sensed acceleration of the probe, the spin rate, and the off-vertical angle estimation. The sensed acceleration of the probe during the pilot and main deployments is shown in Figure 6.

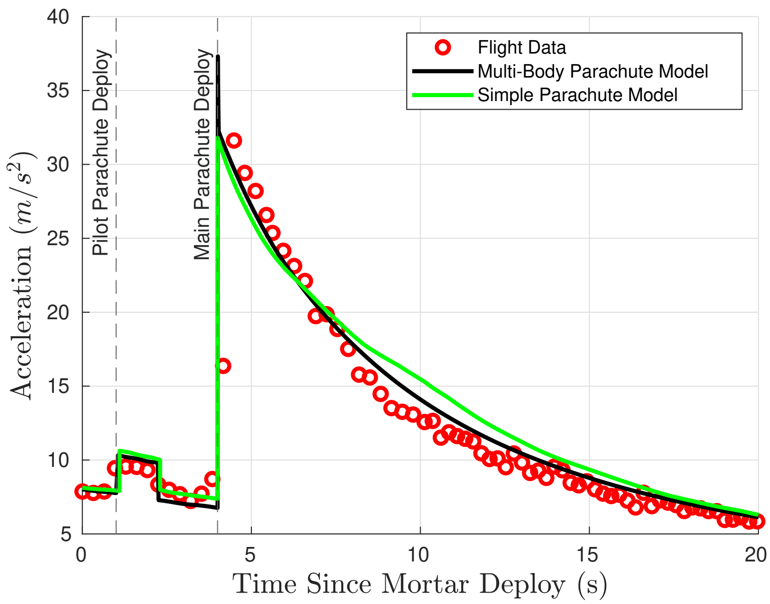

Fig. 6 Acceleration Comparison with the Flight Data at Pilot and Main Deployment

The flight data shows good agreement with the multi-body simulation, with small differences around the interface of configuration changes, like pilot or main deploy. Although the new implementation of the parachute increases the fidelity of the system, there is a level of transience that is very difficult to model without tuned models for each of the subsystems. Namely, the parachute inflation model and the bridle line models are both lacking the very finely tuned inputs that would be necessary to get a better prediction for the main parachute inflation.

Another key configuration change takes place about thirty seconds after main deploy in the form of the heatshield separation. Due to the heatshield constituting a large portion of the total mass of the system, about 25%, the system experiences a sharp acceleration at the event. It should also be noted that the separation has been included in the simulation as a step in mass properties and aerodynamics, without any uncertainties related to delays or specifics of the ejection mechanism. The acceleration spike is shown in Figure 7.

The flight data is not a fine enough resolution to resolve the transience caused by the instantaneous mass change. In the multi-body simulation, a sharp change in mass properties causes an elastic response on the parachute lines that leads to a very high acceleration noted right after that occurs. The extent of the resulting response, with a very high peak acceleration value, is unknown. The driver of the uncertainty around the peak value is the bridle line properties, which were estimated using the Dragonfly model values as a starting point. Additionally, there is no offloading model included in this analysis, which would be specifically aimed at the dynamics of the parachutes when a large mass property step occurs [12].

An observation in the flight data was that the spin rate was the opposite of the prediction. As discussed in the last paper, this was found by an ESA team to be a product of an aerodynamic interaction between the probe and the instrumentation package [13]. Using a set of aerodynamic coefficients from that paper and tuning the damping parameters, a close match was shown between the simulation and the flight data. The match between the multi-body simulation and the flight data can be seen in Figure 8.

With the tuned damping parameters, there is shown to be fairly close convergence to the flight data in the spin rate output. There are differences in the flight data that can be attributed to the cause of the direction of the spin being an aerodynamic interaction between instrumentation packages, which are not modeled in the simulation. The spin rate results come purely from the mixture of rolling moment and damping coefficients that have been taken from the paper

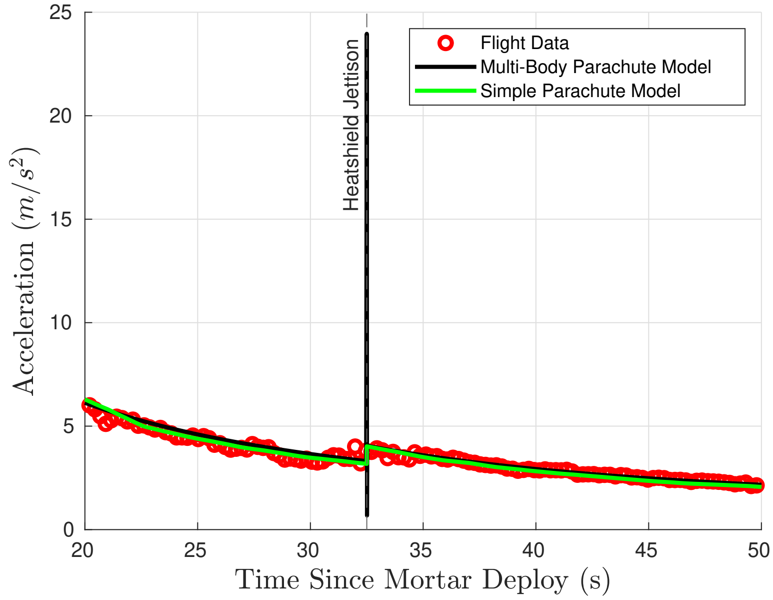

Fig. 7 Acceleration Comparison with the Flight Data at Heatshield Jettison

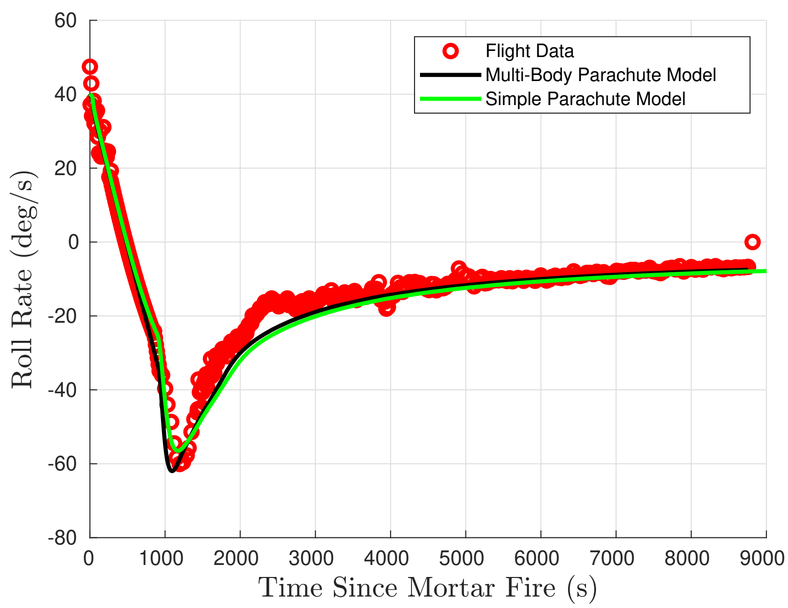

Fig. 8 Acceleration Comparison with the Flight Data

and tuned. Of note is that there is a dependence on which parachute model is being used due to changes in dynamics that are caused by the parachute as an independent body. This leads to differences between the simple parachute model and multi-body parachute model, shown in Figure 8.

B. Triple Bridle Metrics

The implementation of the parachute as a separate body allows for that vehicle and the probe to move semi-independently constrained by the elastic bridle lines. Key metrics of interest can be calculated from the multi-body simulation, including the parachute dynamics, when the bridle lines slack, line forces, and the pull angle of the parachutes relative to the probe, defined as the off-vertical angle of the parachute center of volume from a line centered at the top of the backshell and pointing straight aft. The line forces are calculated by applying the forces and moments generated by the parachute to the triple bridle confluence point. Since the lines act as spring- damper systems, described in Equation 1, the forces effect the probe through those lines. This can also be used to estimate the loads imparted on the pieces of parachute hardware, such as the triple bridle attachments and swivel.

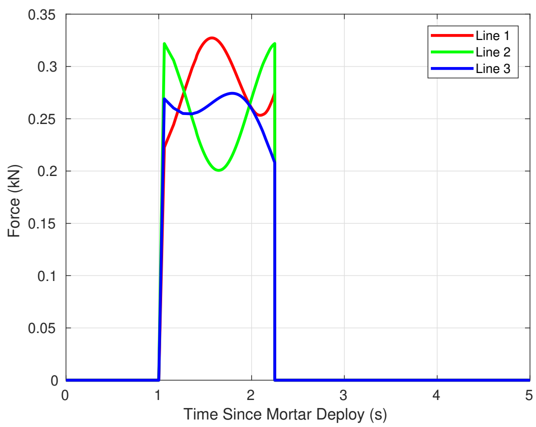

(a) Pilot Parachute Line Forces

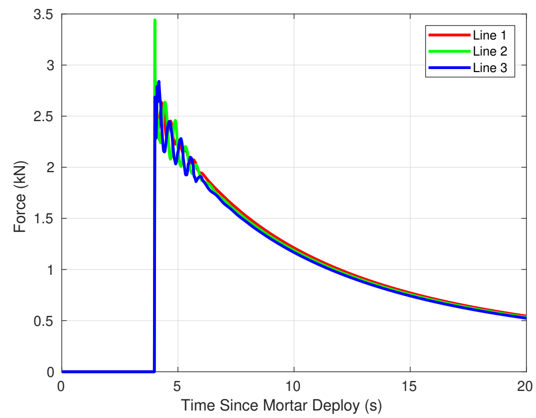

(b) Main Parachute Line Forces

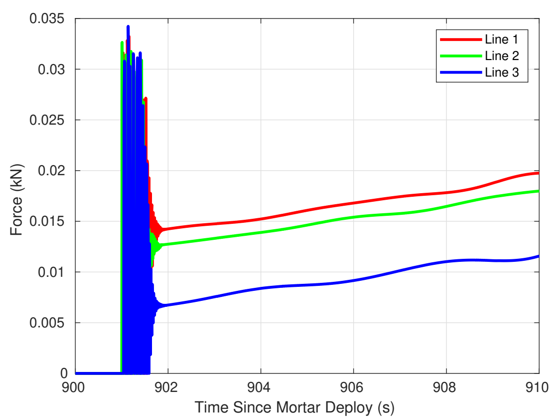

(c) Stabilizer Parachute Line Forces

Fig. 9 Parachute Line Forces During Deployment

In Figure 9(a), the pilot parachute's line forces are shown. Notably, this parachute is mainly used to pull out the main parachute, leading to only about 1.2 seconds between inflation and line cut. The small time that that parachute is under loading leads to the system not damping before line cut. The main parachute line forces, Figure 9(b), shows a sharp increase in forces, notably the largest force seen throughout the trajectory, with a couple of seconds of damping before decreasing. The stabilizer parachute line forces, shown in Figure 9(c), show an elastic response to the change in configuration from main to stabilizer.

The pull angle is calculated as the off-vertical angle of the parachute center of volume from a line centered at the top of the backshell and pointing straight up from that location. These parameters give insight into the mode of the parachute dynamics, as well as the state of the lines. The pull angle describes how the entry vehicle or probe is moving relative to the parachute, which will generally be flying at its prescribed trim angle. The reason for this being a useful metric is that the mode of the parachute can be diagnosed using a combination of both the pull and nadir angles. An example of this is a low pull angle and large oscillations in nadir angle being indicative of a pendulum mode.

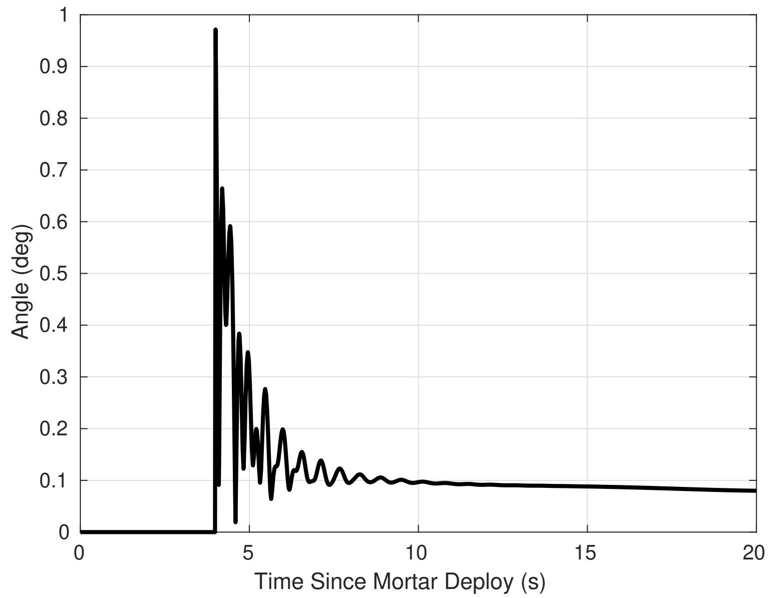

Fig. 10 Pull Angle During Main Parachute Deployment

Figure 10 shows the resulting pull angle for the main parachute, which exhibits the highest angles of the trajectory during inflation. The very low pull angles shown during the trajectory are most likely due to the dynamics of the entry vehicle being dominated by the parachute, with the probe generally staying in line with the parachute center of volume. A reason for this is that the trim angle was set to be very low. Since that value was not known, it was inferred to be near zero, which required a shift in the values in each parachute's aerodatabase. There is uncertainty around this assumption, including heritage in other models. Non-zero trim angles are used in the other missions that have been cited, including MSL, Mars 2020, and Dragonfly. A piece of forward work could be to determine the trim angle, although it would most likely be necessary to have in hand the entire aerodatabase to obtain that knowledge.

Using the line forces, the line slack events can be determined. Line slacks are defined as events in which the relative location of the parachute with respect to the probe lead to a line, or lines, not supporting any of the parachute load. This is mainly due to high pull angles leading to the distance between a line's attachment point and the center of volume of the parachute being less than the stretched length of that line. The line slacking events mainly occur around changes in configuration, such as parachute deployments or separation events.

In Figure 11, the slack state is an output flag for whether the line is slacked, with a 0 being a line in tension and a 1 denoting a slacked line. The definition for a slacked line is when the distance between the two connection point is less than the nominal distance, causing the tension-only spring model to not carry any load. These are most common around changes in configuration, with a small time window showing consistent line slacks right after stabilizer deployment. Additionally, since these slacks occur during very low pull angles, the resulting behavior is thought to be an elastic response to the configuration change. A reason that the line slacks are used as a metric in this paper is due to the hypothesis in Ref. [14] that some of the tilt angle motion was caused by a wrist mode behavior or by lines slacking and reloading. While this metric is heavily dependent on using the correct stiffness and damping terms, the current prediction shows that there are not frequent occurrences of the line slacks. With the low pull angles shown in Figure 10, the assertion is that the current simulation does not predict a wrist mode on the parachute.

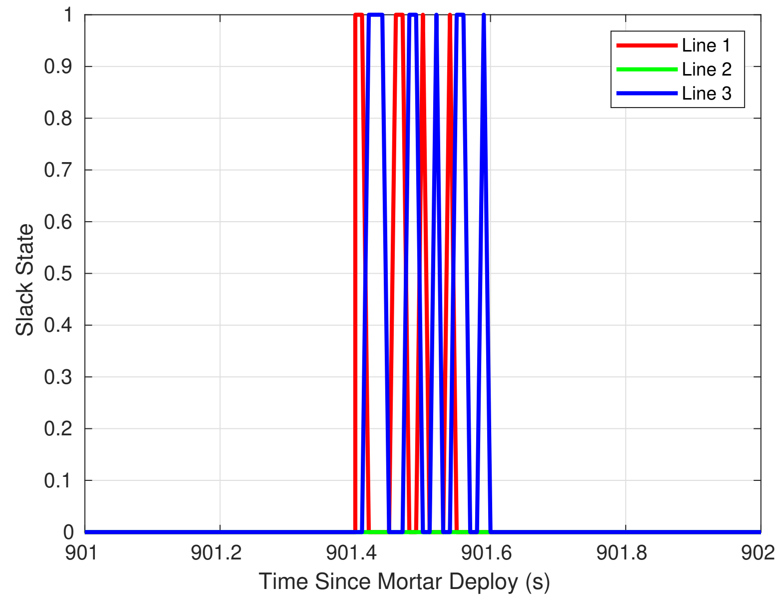

Fig. 11 Stabilizer Parachute Line Slacks

C. Probe Dynamics

The implementation of the multi-body parachute model was aimed at addressing the question of whether the results using the simple parachute model were caused by the parachute model or is a response to the atmosphere model. The most clearly sensitive parameter that has been shown is the nadir angle, so that will be used as the primary comparison tool in this section. The comparison between the two models is important because it shows whether or not the multi-body model has a large effect on the nadir angle.

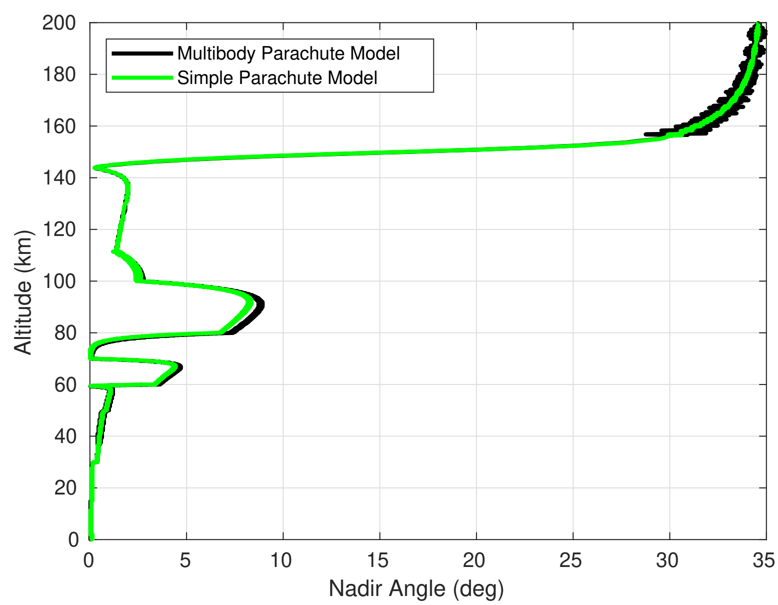

Fig. 12 Nadir Angle Comparison

Figure 12 shows the comparison of the nadir angle under the two different parachute models. The simple parachute model and multi-body model show very good agreement when the gusts are turned off. The nadir angle shows slightly higher values in the altitude bands where the wind causes those values to increase. These increases were noted in the last paper (Ref. [3]), with the noted cause being changes in wind magnitude.

It is important to note that for these nominal cases, the gusts are not modeled. When the perturbations are turned on, the results follow the same general trends due to the steady state winds, just with more noise. The multi-body results follow the same trend as the simple parachute model results that were included in the last paper, with the multi-body results shown in Figure 13.

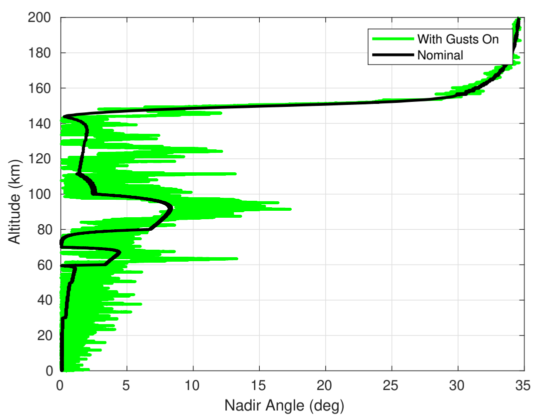

(a) Nadir Angle Profile Gust Comparison with Simple Parachute Model

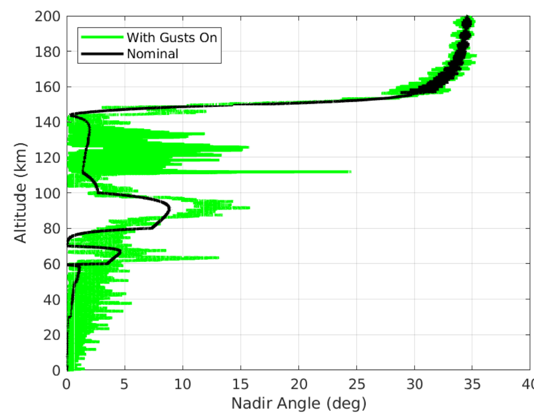

(b) Nadir Angle Profile Gust Comparison with Multi-body Parachute Model

Fig. 13 Nadir Angle Profile Gust Sensitivity

Analysis conducted in Reference [14] gives insight into how the sensor measurements have been pieced together. The metric contained in the work that is most comparable to the nadir angle is the tilt angle, which has been measured using the Automatic Gain Control telemetry from the radio receiver, contained in Figure 8 of Reference [14]. That plot contains the raw data and a curve fit through the data. The curve fit has been taken for comparison in Figure 14.

For the first set of data, Figure 14, the simulation data shows general agreement. The original data set is shown to be noisy, with a large range of values shown in the original figure. The tilt angle is shown to increase in a similar pattern to the simulation results between 1000 and 1500 seconds, although in a lower magnitude. The uncertainty related to the data set can explain some of that difference, with values in the data set showing nearly 20 degrees of tilt in that same region. The tilt data shows a peak at about 1650 seconds that matches the approximate shape of the simulation data peak at about 1850 seconds, indicating a timing difference. Another work, presented in Reference [15], presents another methodology for measuring the off-vertical angle of the probe during descent. Images that were taken during descent were used to measure a pitch angle, referenced as the angle formed by the z-axis presented in Figure 3 and the local horizontal. For the comparison, the nadir angle output by the simulation is always a positive angle so the absolute value of the pitch angle is used for this comparison.

For the DISR data contained in Reference [15], there is a lack of data to draw a firm conclusion on. The simulation data largely bounds the data, shown in Figure 15, although the data is not widely available in the portions of the trajectory that show the higher nadir angles.

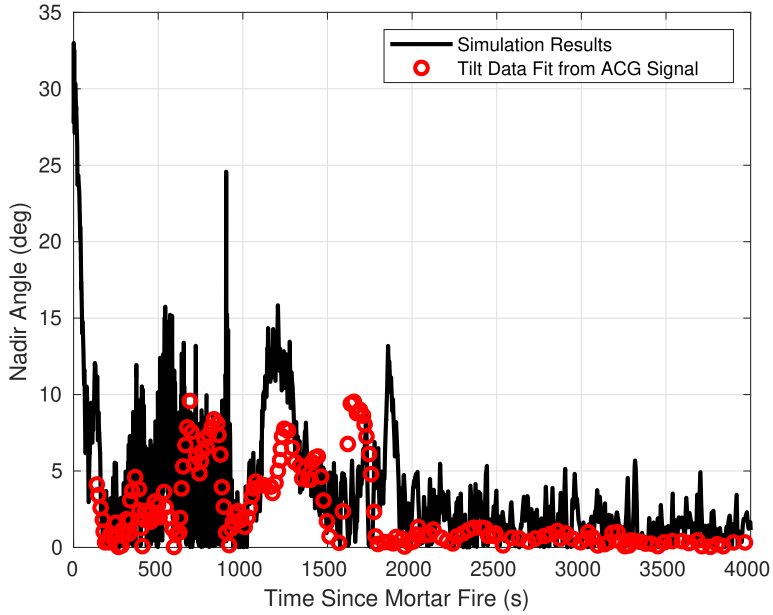

Fig. 14 Nadir Angle Comparison with Tilt Data Derived in Reference [14]

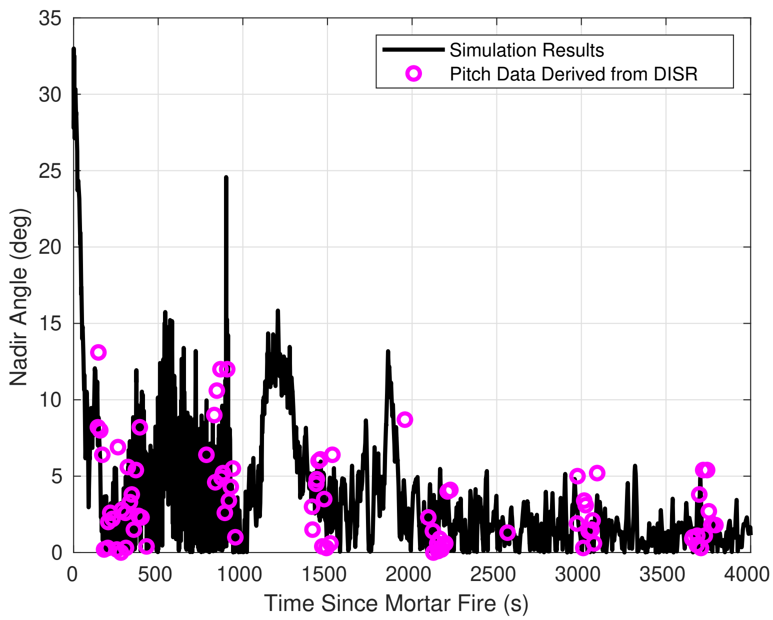

Fig. 15 Nadir Angle Comparison with Tilt Data Derived in Reference [15]

A Monte Carlo simulation was run with the intent of identifying a landing ellipse when only the atmospheric properties are dispersed, including the density, temperature, winds, and gust profiles. Other parameters are not dispersed during this analysis. The landing ellipse for this Monte Carlo, as well as the same set of results using the simple parachute model, are shown in Figure 16.

The landing footprint shown in Figure 16(b) shows a very similar set of results to Figure 16(a), outlining that the simple parachute model is reasonable when determining the bulk trajectory of the vehicle. The nominal trajectory shows

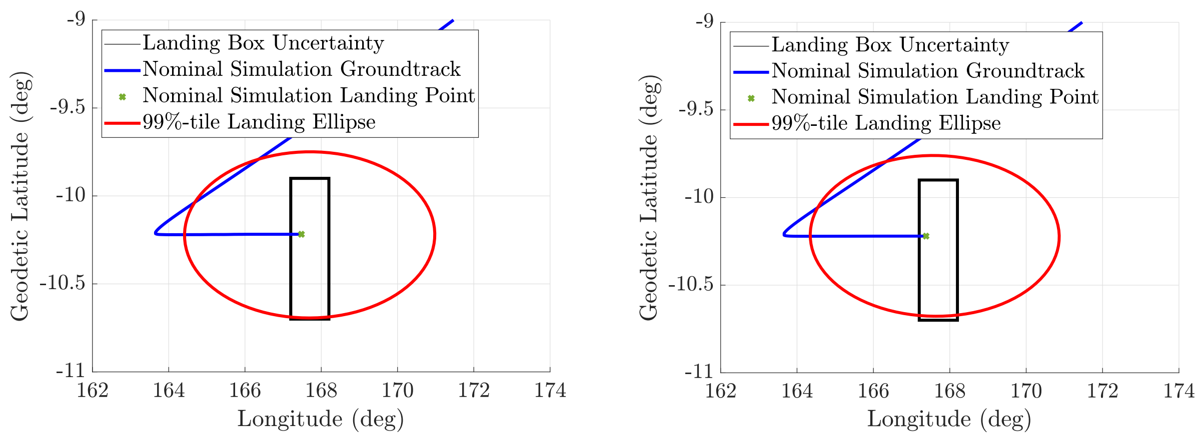

(a) Landing Footprint with Simple Parachute Model

(b) Landing Footprint with Multi-Body Parachute Model

Fig. 16 Landing Footprint Comparison

a touchdown location within the landing uncertainty provided by Ref. [16] using initial states that are aligned with analysis directly in the aftermath of the Huygens descent [17].

V. Conclusion

This paper functions as an extension to prior work presented in Ref. [3] and is aimed at filling a gap in the analysis that was related to the effect of the Dragonfly atmosphere model on the attitude dynamics. In the prior work, a period of elevated nadir angles could be directly traced back to changes in the slope of the zonal wind profile. The results of the analysis conducted in this paper show that comparable flight data can be reasonably predicted by the nadir angle output of the simulation when the gust model is turned on. Additionally, the landing ellipse in the Monte Carlo analysis was shown to give results that matched the estimation of the final landing zone of Huygens.

A conclusion that can also be drawn from this analysis is that the system is not sensitive to the parachute model. The reasoning for the lack of difference between the models is most likely due to the parachute static aerodynamics being based around a zero degree trim angle. More work could be conducted to determine the actual trim angle for each of the parachutes to ascertain the sensitivity of the system to that parameter. However, the metrics that were analyzed throughout this paper showed that the added complexity of the multi-body parachute model did not lead to large differences in the results. The purpose of testing the multi-body parachute model in the simulation was to isolate the reason for the elevated nadir angle and, with multi-body results showing comparable behavior to the simple parachute model, the reasoning for that difference is most likely caused by the zonal wind profile.

Additionally, predicted parachute results have been output to give insight into the behavior of the parachute during the descent. The low pull angle and low variance in nadir angle shows that the parachute is not in a wrist or pendulum mode. Parachute line properties are also output to predict the line slacking events and determine the chute dynamics during the flight. The lack of information over these models leads to uncertainty in the results. Although the lines are made of the same material, the material properties of composites are also based on parameters that are not known and will have a large effect on those results. The results of this portion of the analysis can be used to inform answers to questions on whether line slacks were the cause of some of the recorded flight data that is presented in Reference [14].

The results of the analysis shown in this paper are most specifically aimed at reconciling the results with the atmosphere model. Although the results show agreement with the comparable data, there are still some differences, namely the magnitude of the nadir angle between 1000 and 1500 seconds and the timing of the next nadir excursion. These two small differences are the most notable and could be examined to ascertain the timings and altitudes of zonal winds shifts. Further work could involve directly examining the sensitivity that the system has to zonal wind changes, and whether those changes could be used to reconcile those differences.

Acknowledgments

The authors would like to thank the Dragonfly team who provided feedback for the development of the flight mechanics simulation. The authors would also like to thank Justin Shafner, Giovanny Guecha-Ahumada, Ralph Lorenz, and Daniel Goucheanaur for their help and feedback during the development of this work.

References

[1] Lorenz, R. D., Turtle, E. P., Barnes, J. W., Trainer, M. G., Adams, D. S., Hibbard, K. E., Sheldon, C. Z., Zacny, K., Peplowski, P. N., Lawrence, D. J., et al., "Dragonfly: A rotorcraft lander concept for scientific exploration at Titan," *Johns Hopkins APL Technical Digest*, Vol. 34, No. 3, 2018, p. 14.

[2] Williams, R. A., Lugo, R. A., Marsh, S. M., Hoffman, J. A., Shidner, J. D., and Aguirre, J. T., "Enabling Thread Safety and Parallelism in the Program to Optimize Simulated Trajectories II," *AIAA SciTech 2023 Forum*, 2023, p. 0148.

[3] Pensado, A. R., Robb, C., Winski, R. G., Williams, J. W., Belair, M. W., and Lorenz, R. D., "Assessing Huygens Probe Entry, Descent, and Landing at Titan Simulation using Dragonfly Atmosphere Model," *AIAA SCITECH 2025 Forum*, 2025, p. 2238.

[4] Kazeminejad, B., Atkinson, D. H., Pérez-Ayúcar, M., Lebreton, J.-P., and Sollazzo, C., "Huygens' entry and descent through Titan's atmosphere—Methodology and results of the trajectory reconstruction," *Planetary and Space Science*, Vol. 55, No. 13, 2007, pp. 1845–1876.

[5] Pensado, A. R., Winski, R. G., Williams, J. W., and Robb, C., "Dragonfly Mission Entry and Descent Modeling and Simulation Overview," *AIAA SCITECH 2025 Forum*, 2025, p. 2237.

[6] Lebleu, D., "Huygens Probe/Probe Reference Data for Post Flight Analysis," Tech. rep., 2005.

[7] Cruz, J. R., Way, D., Shidner, J., Davis, J. L., Powell, R. W., Kipp, D., Adams, D. S., Sengupta, A., Witkowski, A., and Kandis, M., "Parachute models used in the Mars Science Laboratory entry, descent, and landing simulation," *AIAA Aerodynamic Decelerator Systems (ADS) Conference*, 2013, p. 1276.

[8] Dutta, S., Karlgaard, C. D., Tynis, J. A., O'Farrell, C., Sonneveldt, B. S., Queen, E. M., Bowes, A. L., Leylek, E. A., and Ivanov, M. C., "Advanced supersonic parachute inflation research experiment preflight trajectory modeling and postflight reconstruction," *Journal of Spacecraft and Rockets*, Vol. 57, No. 6, 2020, pp. 1387–1407.

[9] Cruz, J. R., and Snyder, M. L., "Estimates for the aerodynamic coefficients of ringsail and disk-gap-band parachutes operating on Mars," *24th AIAA aerodynamic decelerator systems technology conference*, 2017, p. 4055.

[10] O'Farrell, C., and Clark, I. G., "Reconstructed Performance of Mars 2020 Parachute Decelerator System," *Journal of Spacecraft and Rockets*, Vol. 61, No. 5, 2024, pp. 1313–1328.

[11] Yelle, R., Strobel, D., Lellouch, E., and Gautier, D., "Engineering models for Titan's atmosphere," *Huygens: Science, Payload and Mission*, Vol. 1177, 1997, pp. 243–256.

[12] Polutchko, R. J., "Free-Flight Test Results of Scale Models Simulating Viking Parachute/Lander Staging," Tech. rep., 1973.

[13] Lebreton, J.-P., and Leroy, A., "Huygens Close-out Activities Final Technical Report," Tech. rep., 2020.

[14] Lorenz, R. D., "Decoding the Descent Dynamics of the Huygens Probe," *2022 IEEE Aerospace Conference (AERO)*, IEEE, 2022, pp. 1–14.

[15] Karkoschka, E., Tomasko, M. G., Doose, L. R., See, C., McFarlane, E. A., Schröder, S. E., and Rizk, B., "DISR imaging and the geometry of the descent of the Huygens probe within Titan's atmosphere," *Planetary and Space Science*, Vol. 55, No. 13, 2007, pp. 1896–1935.

[16] Lebreton, J.-P., Witasse, O., Sollazzo, C., Blancquaert, T., Couzin, P., Schipper, A.-M., Jones, J. B., Matson, D. L., Gurvits, L. I., Atkinson, D. H., Kazeminejad, B., and Pérez-Ayúcar, M., "An overview of the descent and landing of the Huygens probe on Titan," *Nature*, Vol. 438, No. 7069, 2005, pp. 758–764. https://doi.org/10.1038/nature04347, URL https://www.nature.com/articles/nature04347, publisher: Nature Publishing Group.

[17] Striepe, S. A., Blanchard, R. C., Kirsch, M. F., and Fowler, W. T., "Huygens Titan probe trajectory reconstruction using traditional methods and the program to optimize simulated trajectories II," *17th AAS/AIAA Space Flight Mechanics Meeting*, 2007.